Layout pattern analysis and coverage evaluation in computational lithography

YAOBIN FENG,[1] ZHIYANG SONG,[1] JIAMAN LIU,[2] ZHIQIN LI,[2] FENG YANG,[2] HAO JIANG,[1,3,4] (iD) AND SHIYUAN LIU[1,3,5] (iD)

[1]*State Key Laboratory of Digital Manufacturing Equipment and Technology, Huazhong University of Science and Technology, Wuhan 430074, China*
[2]*Brion Technologies (Shenzhen) Co., Ltd., Shenzhen 518054, China*
[3]*Optics Valley Laboratory, Wuhan 430074, China*
[4]*hjiang@hust.edu.cn*
[5]*shyliu@hust.edu.cn*

Abstract: In advanced semiconductor technology nodes, the model accuracy of optical proximity correction (OPC) is the key for integrated circuit (IC) chip mask tape out, yield ramp up, and product time-to-market. An accurate model means a small prediction error for the full chip layout. As the full chip layout usually has large pattern variety, an optimal pattern set with good coverage is desired during the model calibration process. Currently, no existing solutions can provide the effective metrics to evaluate the coverage sufficiency of the selected pattern set before a real mask tape out, which may potentially cause higher re-tape out cost and product time-to-market delay due to the multiple rounds of model calibration. In this paper, we construct the metrics to evaluate the pattern coverage before any metrology data is obtained. The metrics are based on either the pattern's intrinsic, numerical feature representation, or its potential model simulation behavior. Experimental results show a positive correlation between these metrics and lithographic model accuracy. An incremental selection method is also proposed based on the pattern simulation error. It reduces up to 53% of the model's verification error range. These pattern coverage evaluation methods can improve the efficiency of OPC model building, and are, in turn, beneficial to the whole OPC recipe development process.

1. Introduction

During the semiconductor manufacturing process, lithography is used to transfer the patterns from an integrated circuit (IC) design inlayed on a photomask to the semiconductor wafer. As the dimension of the design shrinks to be smaller than the wavelength of the light source, lithography printing suffers from optical proximity effects and cannot yield the sufficient printing resolution without modifications to the raw designs. This modification process that compensates for these optical proximity effects is called optical proximity correction (OPC) [1–4]. This design-to-mask transformative process requires an accurate lithography model in order to simulate the whole lithography process (Fig. 1) [3] and to drive the design correction. Typically, a lithography model takes a predefined mathematical form with multiple open parameters. The model form may be derived from optical/physical/chemical processes [5–8] or constructed by a neural network [9–12]; while the open parameters associated with the model form need to be determined through a calibration process [13].

As technology nodes shrink in size, the error budget for the lithography process deceases, and the lithography model's accuracy targets become increasingly challenging to achieve. An over-fitted model, which yields good performance on the calibration pattern set, may predict poorly on different patterns that show up in real chip designs. An inaccurate model tends to result in wafer defects that are not predicted by OPC verification, thus leading to lower-than-expected wafer yield once it goes into high-volume manufacturing.
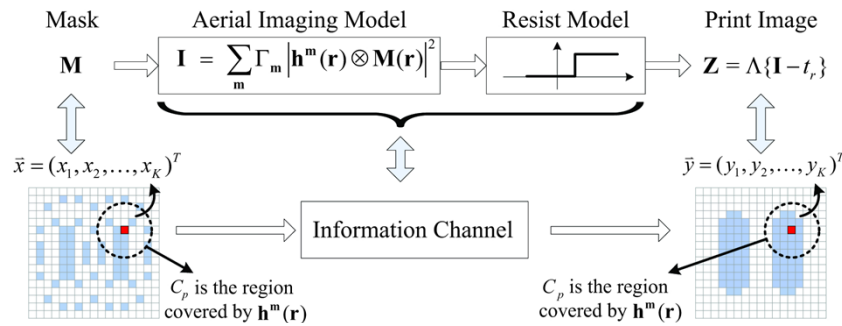
Fig. 1. Mathematical illustration of lithography process simulation.

A pattern set used for calibration with sufficient pattern coverage is an area that becomes increasingly important as model forms become more and more complicated. A common practice is to set up the calibration patterns based on geometrical properties according to an engineer's experience. Generally, regular line/space or contact array patterns that have a certain range of critical dimension (CD) are selected with the intent to cover a large portion of the pattern space. Patterns selected from real chips are also added to provide additional design information for model calibration, while such manual selection suffers from high labor-intensity and low consistency. To address these issues, an image-based pattern selection (IBPS) [14] method has been demonstrated to automatically and smartly select patterns from a full real chip using feature vectors.

Here the feature vector (FV) is defined as an abstracted, numerical representation of the patterns, which is formed from the patterns' aerial images. Feature vectorization is a widely-used technique in the computational lithography field for pattern selection [15–17] and hotspot detection [18–20]. Typical FVs which originate from the design layouts or the pattern clips after OPC generally contain only geometrical information [21,22]. In the IBPS method, FVs are converted from aerial images of pattern clips. In this way, all optical effects in the lithography model are considered when constructing the feature space with better physical correspondence.

Although IBPS method has been demonstrated in previous literature to improve the pattern coverage compared to a random selection, we still need to have methods to assess and quantify the pattern coverage in order for industry users to put together a set of calibration patterns that can best represent the design as the eventual goal. In this paper, we introduce the FV-based and simulation-based methods to analyze the coverage of a sub pattern set and evaluate their correlation to a model prediction's performance. Feature vectors can enable one to check the relationship among patterns which then allows one to evaluate the pattern coverage given the overlapping status of a selected pattern subset to the full set of patterns within the feature space. This statistical evaluation method specifically focuses on the diversity of a selected pattern set. Its results suggest a positive correlation between the FV based metrics and the average model accuracy across a full pattern set. However, model accuracy can also be sensitive to a few critical patterns which could severely damage the model's prediction accuracy. This phenomenon is difficult to be well captured by FV based metric alone, so the simulation based metric is introduced in this paper for complementation. The simulation-based method constructs the metrics by performing a model inaccuracy evaluation using a simulation-based flow mimicking the model calibration. Its metrics focus on the patterns with high sensitivity and criticality to the lithography model calibration process. As a result, a strong positive correlation is exhibited between these metrics and the model's measured error range. It is also shown that the minor critical patterns can strongly deteriorate these metrics, leading to a poor coverage score. On the contrary, guided by these metrics, one can optimize the calibration pattern set by adding back into it the most

critical patterns via an incremental selection methodology. Incremental selection simply picks the top ranking patterns that limit the simulation-based coverage score. This is done prior to the cycle of mask making, wafer exposure and metrology data collection, which can significantly reduce the overall turnaround time. The result verifies that incremental selection improves the final lithography model's performance on those remaining critical patterns without sacrificing the accuracy of the pattern majority. It should be noted that FV-based method is recommended in the first round of OPC iterations as it is decoupled with resist model calibration, has short runtime, and high stability; while the simulation-based method, albeit with slow runtime, is more preferable and less expensive when being adopted in the later rounds as there already obtained a baseline model from previous rounds. It is expected that reasonably using the pattern selection and coverage evaluation methods at different stages in the model calibration flow, as shown in Fig. 2, can benefit the lithography model accuracy. In the flowchart, green blocks indicate the two pattern coverage evaluation methods, and the incremental pattern selection method introduced in this paper.
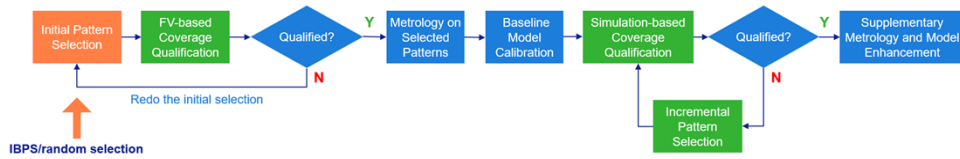

Fig. 2. Flow chart of pattern selection and coverage evaluation methods in the model calibration flow.

2. Pattern coverage evaluation methods

2.1. *FV based pattern coverage evaluation*

Pattern diversity within a calibration pattern set is very important for model accuracy. When the calibration pattern set cannot represent all the pattern types in a real chip, the model prediction power will decrease significantly on certain patterns. The FV based method evaluates the pattern coverage in the feature space and focuses on pattern diversity. Three primary procedures which are used within this methodology include FV extraction, pattern clustering on the full set of patterns, and the pattern coverage calculation.

2.1.1. Feature vector extraction

In computational lithography, aerial images are generally obtained by applying an optical model to a mask layer. The intensity of an aerial image in the lithography system is given by [22]:

$$I(\hat{x},\hat{y}) = \int\!\!\!\int_{-\infty}^{+\infty} J(\hat{f},\hat{g}) \left[\left| \int\!\!\!\int_{-\infty}^{+\infty} H(\hat{f}+\hat{f}',\, \hat{g}+\hat{g}')O(\hat{f}',\hat{g}')e^{-i2\pi(\hat{f}'\hat{x}+\hat{g}'\hat{y})}d\hat{f}'d\hat{g}' \right|^2 \right] d\hat{f}d\hat{g} \qquad (1)$$

where $(\hat{x},\hat{y})$ is the coordinate at the aerial image plane, $(\hat{f},\hat{g})$ is the coordinate at the pupil plane, $J(\hat{f},\hat{g})$ is the source's mutual intensity function, $H(\hat{f},\hat{g})$ is the light propagation function, and $O(\hat{f},\hat{g})$ is the mask spectrum.

Since aerial images simultaneously contain both optical and geometric signatures, they are used instead of polygons to extract FVs through an unsupervised autoencoder model [23–25] as shown in Fig. 3. By doing so, both geometric and optical information are encoded into the FVs.

An unsupervised autoencoder is used in our FV based method to construct the FV space. With a proper design, the autoencoder model can help to find the proper low dimensional manifold
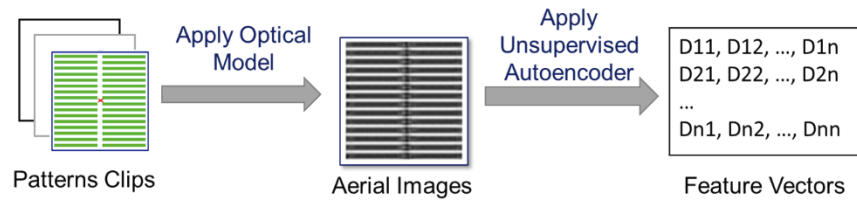
Fig. 3. Illustration of FV extraction.

embedded within the high-dimension space [26]. This is needed to ensure that the data points maintain their structured similarity between the output's low dimensional FV space and the original aerial image in high-dimensional space. The loss function in the autoencoder model, the major component of which is mean square loss, can be mathematically described by the following equation:

$$Loss = \ ||\text{Mask}(f(g(x)) - x)||_2^2 \tag{2}$$

where a customized Mask() function is added into our autoencoder's loss function to highlight the aerial image's centroid region or the physically guided components as shown in Fig. 4. In order to avoid any overfitting risk, the unsupervised autoencoder model is trained with aerial images from all patterns that are extracted from the full layout.
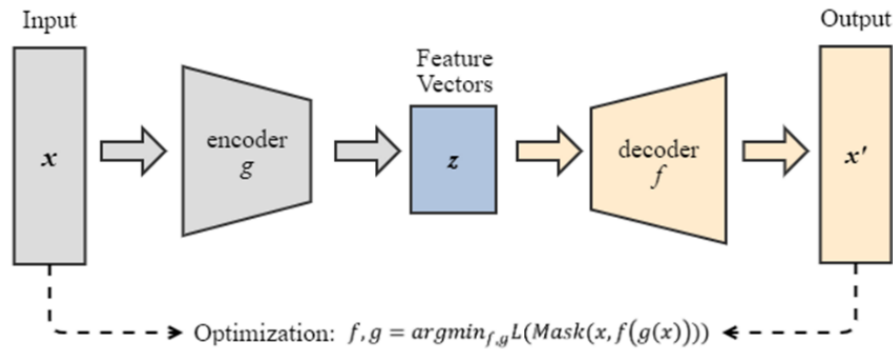

Fig. 4. Autoencoder training. Mask() is the customized function of autoencoder training loss function in our methodology.

Every pattern's FV is output after applying the autoencoder model. The resultant FV dimension is ~1/25 of the raw image's with minimal information loss, which significantly improves the runtime of this FV based method. With certain neural network training to ignore insignificant data by constraining the input/output of network to achieve high structural similarity while have sufficient reduction in the output FV dimension, the significant features in the original aerial images can be enhanced which may benefit the result of the following modules [26]. An example of the encoder training performance in the test case of this paper is shown in Fig. 5. For pattern with maximum encoder loss, the mean pixel-to-pixel difference between input image and recovered image is 0.008 while AI intensity contrast in it is ~0.27, which means average pixel distortion is < 3%. For pattern with minimum encoder loss, the mean pixel-to-pixel difference between input image and recovered image is 0.002 while AI intensity contrast in it is ~0.28, which means average pixel distortion is < 1%.

In the scope of this paper, a Euclidean distance is used to quantify the pattern differences and to generate the relationships between patterns in the FV space. Patterns or images which have higher similarities tend to have smaller FV distances as shown in Fig. 6. In the FV space,
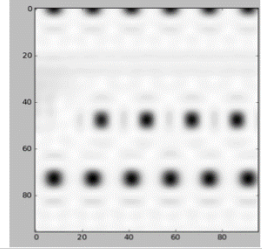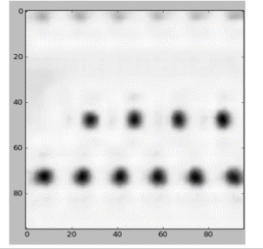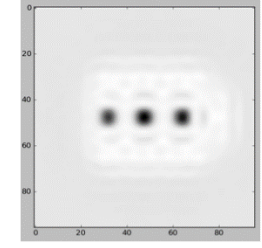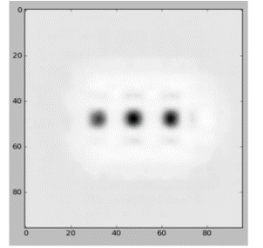
Pattern	Original AI image	Decoded AI image	AE performance
A			Loss (highest): mean diff) = 0.0083427839 Contrast = 0.27 Mean_diff/contrast =3%
B			Loss (low): mean diff) = 0.00215 Contrast = 0.278 Mean_diff/contrast <1%

Fig. 5. Examples of encoder training performance.

a pattern is considered covered if the distance from itself to any selected pattern is less than a distance threshold. The pattern clustering module is designed to provide a solution to define the distance threshold for checking covered and uncovered patterns.

(a) Reference pattern   (b) FV distance = 0.12   (c) FV distance = 0.46

(d) FV distance = 0.88   (e) FV distance = 1.45
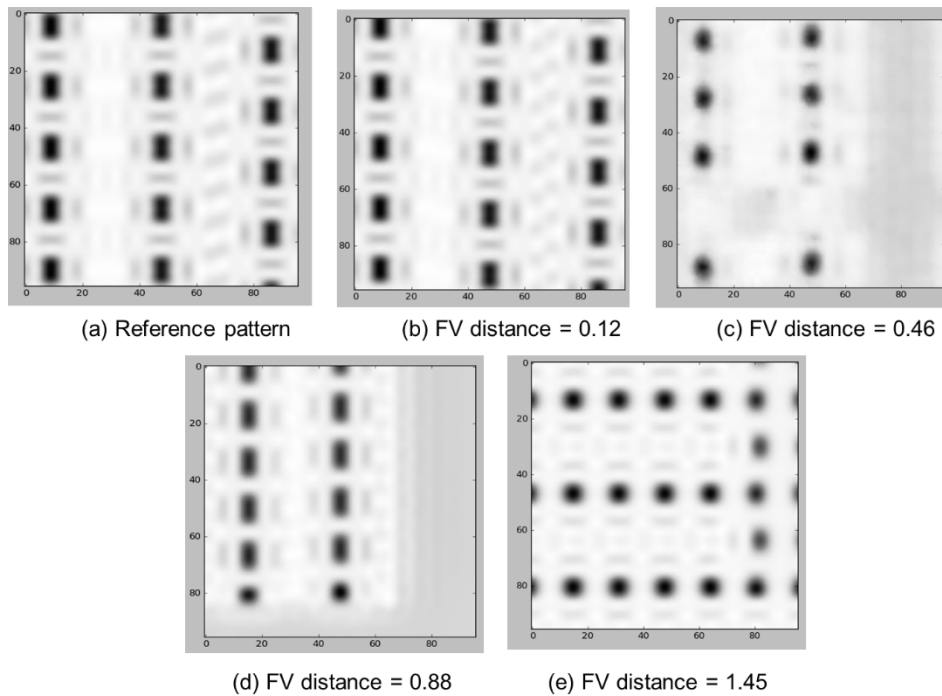
Fig. 6. Illustration of pattern similarity vs FV distance: (a) reference pattern with 96×96 pixels, (b)-(e) are context patterns with similarity decreasing, and the FV distance to reference pattern is 0.12, 0.46, 0.88, and 1.45, respectively.

2.1.2.   Pattern clustering on a full layout

Based on the extracted FVs, pattern clustering is applied on a full pattern set in the way that the separation between each pair of patterns in a cluster is less than a distance threshold. An illustration of pattern clustering is shown in Fig. 7, where principal component analysis (PCA), a dimensionality-reduction method, is applied for visualization purposes.
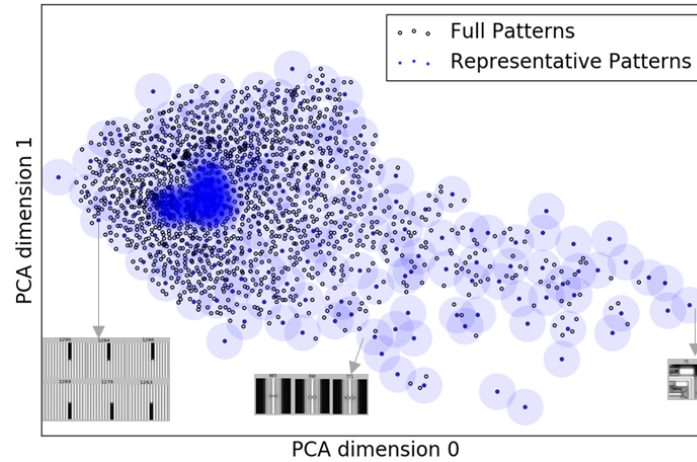

Fig. 7. A 2D illustration of a clustered pattern set in design space. Patterns within the blue circle are in one cluster. The blue circle radius indicates the distance threshold.

Since similar images have small FV distance, the characteristic of pattern similarity in the full pattern set can be recognized with the nearest neighbor distance of the full pattern set. By statistically analyzing the nearest neighbor (NN) distance distribution, e.g., calculating the mean value of the NN distances, a distance threshold of this known space is defined to cluster patterns into different groups. A pair of patterns that are nearer than this distance threshold in the FV space is eligible to be clustered together. The final clustering result is determined by identifying a minimum count of clusters containing all of the patterns. Denoting the number of cluster as N and the maximum pairwise distance of two patterns appearing in the same cluster as R, the clustering behavior can be mathematically described with the following optimization statement:

$$Minimize\ N,\ subject\ to\ R < distance\_threshold \tag{3}$$

This optimization problem can be solved by a greedy algorithm [27,28] to generate the clustering result. The detailed algorithm of greedy algo is listed as following:

```
Greedy (F, C) { // F is full pattern set, and C are representative patterns
    Initialize U = F, C = Ø
    while (U is not empty) {
        N[i] = loop U to collect neighbor in U < distance_threshold
        Pick i with largest count(N[i])
        add i to C
        remove N[i] from U
        }
    return C
    }
```

In real production tape-out process, greedy algo can be too expensive to adopt on a large data set from full chip layout. Thus, distributive computing of greedy algo could be introduced to achieve the result within acceptable runtime.

From the clustering result, one representative pattern set associated with the distance threshold can be obtained for a full pattern set by picking up the centroid pattern from each individual cluster. They can be repeatedly used to evaluate pattern coverage of different selected pattern sets against the full pattern set within the same FV space. It reduces the information redundancy and increases the computational efficiency. And the distance threshold can be used as a criterion to recognize covered and uncovered patterns within the pattern calculation module.

2.1.3. Pattern coverage calculation

A FV based pattern coverage index is calculated by comparing representative patterns to selected patterns. As shown in Fig. 8, a covered pattern means its minimum distance to any selected patterns is less than the distance threshold. The FV based pattern coverage ratio (FV-PCR) is calculated as

$$FV\_PCR = \frac{Covered\,Pattern\,Count}{Total\,Representative\,Pattern\,Count} \tag{4}$$
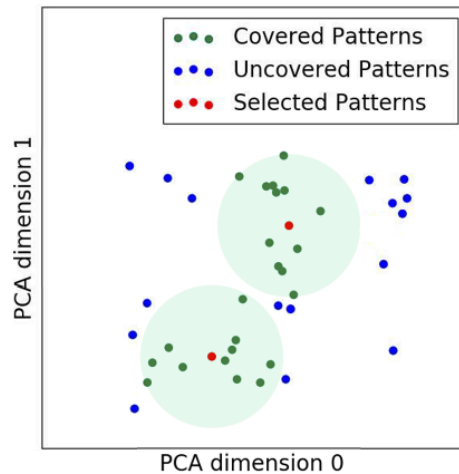

Fig. 8. A 2D illustration of covered patterns in FV space.

The larger ratio indicates better pattern coverage. The FV-PCR's key performance index (KPI) deteriorates when more and more patterns are found to be outside of the distance threshold from that of all of the selected patterns.

One advantage of our FV based pattern coverage evaluation method is that it has the capacity to support full chip calculations with a low runtime cost. In addition, it is flexible and convenient enough to be implemented with different use cases which can make use of the application's KPI.

2.2. Simulation based pattern coverage evaluation

Similar to FV based pattern coverage evaluation method, the simulation based pattern coverage evaluation method could also save the turnaround time and the tape-out cost by improving the pattern coverage to enhance model accuracy and reduce re-calibration iterations. The pattern coverage simulation based method mimics a neural network's model training process. It uses simulated data generated from a baseline physical model, which has an error RMS of 1.99 nm, an error Range of 14.69 nm, and a 3 Sigma of 7.32) as input. In this way, this method can be

applied without the need for real metrology data. This is a benefit since gettering the real, ground truth data comes associated with a rather high portion of the cost when training a model. The overall methodology, metrics design and incremental selection will be introduced in the following sections.

2.2.1.   Methodology

The metrics of our simulation-based method is designed based on model error severity estimation and analysis. Model error severity is estimated by disagreement between the trained neural network model and the baseline physical model from which the neural network model is trained. The flow is shown in Fig. 9(a). Firstly, the existing baseline physical model is simulated on the already selected pattern set to prepare the ground-truth data. Then the neural network model is trained with such data generated from the baseline model's simulation results. By further doing simulation on a full pattern set using both models, the model disagreement errors and associated model severity can be extracted which is used to calculate the simulation-based metrics and drive the incremental selection.
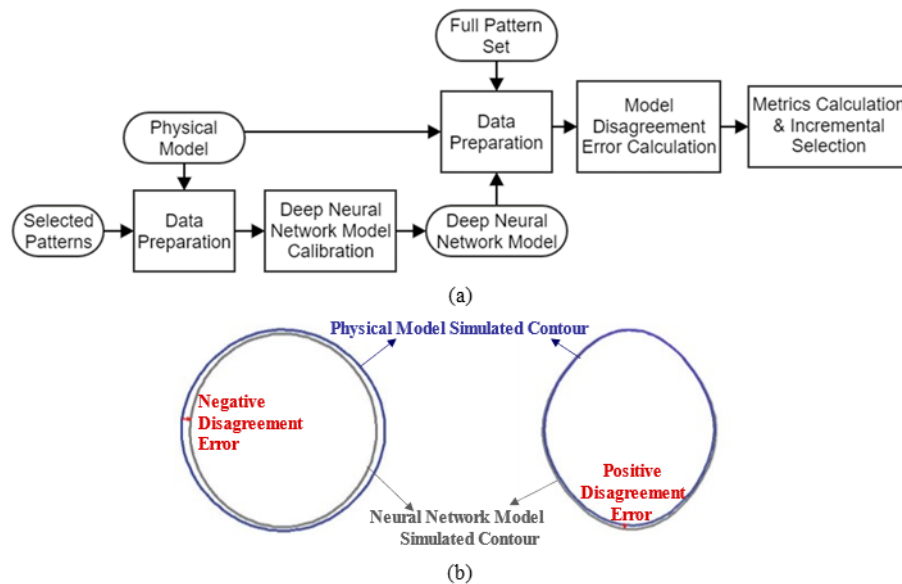

Fig. 9. Simulation based pattern coverage evaluation method: (a) flow, (b) illustration of model disagreement error.

Generally, the model disagreement error can be described as the sum of resist image mismatch between the deep learning model prediction and the baseline model prediction. In practical application, due to specific features derived from resist image such as critical dimension variation (CDV) is a key point, a reduced KPI of CDV is constructed for ranking in this work:

$$pattern\ severity\ =\ rank(\sum CDV(DL\,model,\ baseline\,model)|_{critical\,locations}) \qquad (5)$$

As the constructed neural network is a deep learning network containing > 20 layers and > 5000 neurons, it has stronger fitting power than physical models [29,11]. This means, it can have good predictions not only on those selected patterns that are used for training the neural network but also on those unused but well covered patterns in the full pattern set. This means that larger absolute disagreement errors between the two models applied to the full pattern set can highlight uncovered patterns by the selected patterns. Metrics from the simulation based method are

constructed with the simulated model error result, i.e., model disagreement as described in the following section.

2.2.2. Metrics design

The metrics of the simulation-based method are constructed by statistical analysis of the estimated model errors, including error range and standard deviation of the full pattern set. The error range (Err-R) indicates the maximum positive and minimum negative model disagreement error. The error standard deviation (Err-STD) shows the trend of the overall model disagreement error.

$$Err\_R = \max error - \min error \tag{6}$$

$$Err\_STD = \sqrt{\frac{\sum (error - \overline{error})^2}{N}} \tag{7}$$

Since the neural network model has its original fitting power, we infer that there is no perfect model to have zero model disagreement error even on the selected training pattern set. The residual error, also known as neural network model training error on the selected pattern set, should be taken into account in the pattern coverage metrics design. Thus, the following metrics are designed in this paper as the simulation-based pattern coverage evaluation KPIs.

1. Error range difference ratio (ERDR):

$$ERDR = \frac{Full\,Pattern\,Set\,Err\_R - Selected\,Pattern\,Set\,Err\_R}{Full\,Pattern\,Set\,Err\_R} \tag{8}$$

(2) Error standard deviation ratio (ESDR):

$$ESDR = \frac{Selected\,Pattern\,Err\_STD}{Full\,Pattern\,Err\_STD} \tag{9}$$

In principle, with a smaller error range difference ratio, more unused patterns in the full pattern set are better predicted by the neural network model, thus indicating better pattern coverage. The error distribution reflects the disagreement between the neural network model and the physical model on the overall behaviors of the patterns. As the error standard deviation ratio gets closer to 1, the predication result of the trained neural network model and the baseline physical model on the selected patterns and the full patterns become more similar, indicating better coverage of the selected patterns on the full pattern set.

2.2.3. Incremental selection

Incremental selection optimizes the calibration pattern set by adding those top-ranking patterns in the severity ranking of the full pattern set as shown in Fig. 10. The top-ranking patterns
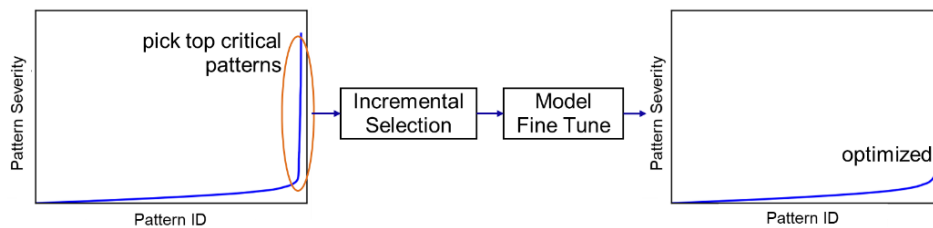

Fig. 10. Conceptual illustration of incremental selection to optimize a selected pattern set.

are critical, unused and uncovered patterns in the original selected set. The originally selected pattern set is optimized by adding these critical patterns, thus approaching better coverage.

The optimization is done before metrology. Incremental selection is proven in the result to improve OPC model accuracy with a shortened turnaround time.

3. Pattern selection and the experimental design

With the pattern coverage evaluation methods, an efficient model calibration flow is shown in Fig. 11. The experiment is designed according to this flow.
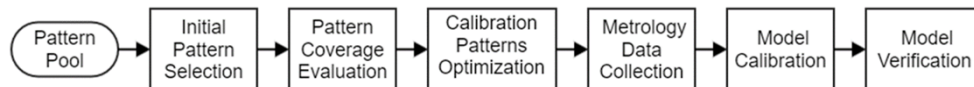

Fig. 11. Model calibration flow.

3.1. Image based pattern selection

As the initial step of the model calibration flow, pattern selection is desired to be applied on a full layout to ensure the model's coverage of a full layout pattern set. Compared to random selection, IBPS automatically selects patterns from a full layout with larger pattern diversity, thus achieving higher pattern coverage. In addition, IBPS reduces the efforts of manual pattern review and thus increases the engineering efficiency [14].

IBPS is a machine learning technique to select patterns that considers FV diversity. The initial input of IBPS is a full chip layout. The output of IBPS is the selected patterns that can represent the pattern diversity of the full chip layout. IBPS undergoes three primary steps as shown in Fig. 12, unique patterns extraction, FV extraction, pattern grouping and down sampling.
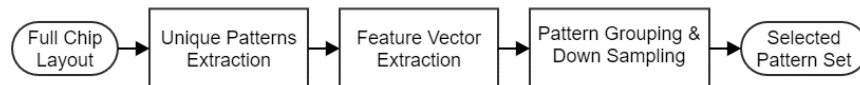

Fig. 12. Image based pattern selection flow.

Unique patterns refer to geometrically unique patterns when extracted within a defined region which considers the proximity effect. Geometrically unique patterns mean the exact matching of each polygon and vertex. In general, unique patterns are extracted from a full chip layout to reduce the pattern redundancy and increase the efficiency. Feature vectors are extracted from aerial images using an unsupervised auto-encoder method. The pattern grouping module arranges patterns with similar FVs into one group meanwhile separate patterns with different FVs. In the down sampling module, certain number of patterns from all groups are selected to ensure better coverage on pattern geometry, lithography optical behavior and other model sensitive features.

As shown in Fig. 13, which schematically illustrate the distribution of 300 selected patterns in design space, IBPS generally has an even selection of patterns regardless of pattern density in the FV space while random selection is prone to select more patterns in the high population region. Under such a circumstance, IBPS can achieve a more diverse selection and thus better pattern coverage than random selection.

3.2. Experimental design

In this paper, we demonstrate two methods to evaluate pattern coverage of a calibration pattern set in a DUV memory case with an NA of 1.3, the feature size of which ranging from 80 nm to 120 nm.
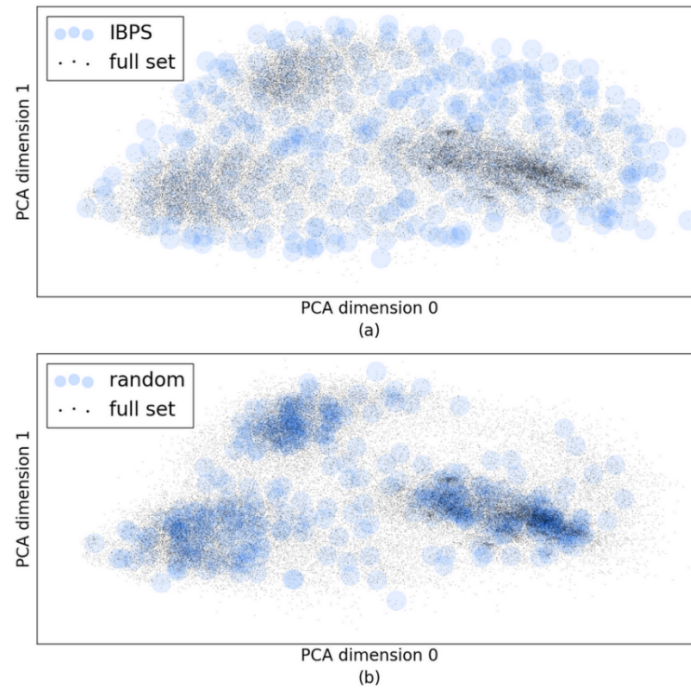
Fig. 13. A 2D illustration of the distribution of 300 selected patterns in design space: (a) IBPS shows a uniform selection thus achieving a higher FV coverage index, (b) random selection selects patterns in high populated regions. The blue circle radius visualizes the distance threshold used in the FV pattern coverage evaluation method.

In order to prove the validity of the pattern coverage evaluation method and the corresponding pattern coverage metrics, random pattern selection and IBPS methods are implemented on a real full chip layout using a contact layer with different selected counts to prepare the experimental data as shown in Table 1. All the unique patterns in the real full chip are arranged as a full pattern set for this pattern coverage evaluation.

Table 1. Pattern selection cases for experiment preparation

Case ID	Pattern Selection Method	Pattern Selection Count
Random 100	Random	100
Random 300	Random	300
IBPS 100	IBPS	100
IBPS 300	IBPS	300
IBPS 600	IBPS	600

An incremental selection is applied on IBPS 100, IBPS 300 cases to add the 10 most critical patterns identified by the simulation based method from the unselected pool and optimize them for cases Incremental 110 and Incremental 310. After the pattern coverage evaluation, metrology data for each selected pattern set is collected from an exposed wafer, and one real lithography model is calibrated and verified for each set.

4. Results

The FV based and simulation-based pattern coverage evaluation methods are applied on the experimental cases. Physical models are calibrated with the metrology data of the selected patterns in each case. Ideally, the full pattern set should be used as a verification pattern set. However, there are over 400,000 unique patterns in the layout which are not affordable for metrology. Given a reasonable metrology budget, a 3,000-pattern subset is extracted from all of the unique patterns and are used as the verification pattern set for the experiment.

Model prediction accuracy is used to verify the effectiveness of the two pattern coverage evaluation methods. To quantify the model prediction accuracy, two KPIs (differences between the model predicted contour and the measured contour on wafer) are constructed by statistical analysis of the physical model's verification errors. The first KPI is the root mean square (RMS) of the model verification error, indicating the overall prediction accuracy across the verification patterns. The second KPI is the model verification error range (max error – min error) which shows whether there are particular patterns for which the current model's predication accuracy is sufficient or not. The smaller KPI resultant values obtained are indicative of us achieving better model accuracy.

4.1. FV pattern coverage metric correlates with model accuracy

In general, better design diversity of the calibration pattern set could help achieve a lower error RMS for the calibrated model. As shown in Fig. 14, the FV pattern coverage index shows a positive correlation to the model verification error RMS and range. An increasing FV pattern coverage index corresponds to a reduction in the model verification error RMS, and thus improves the corresponding model accuracy. The full set calibration results, which have an error RMS of 1.61 nm and an error Range of 17.57 nm, largely follows the result, indicating the efficacy of FV pattern coverage metric.
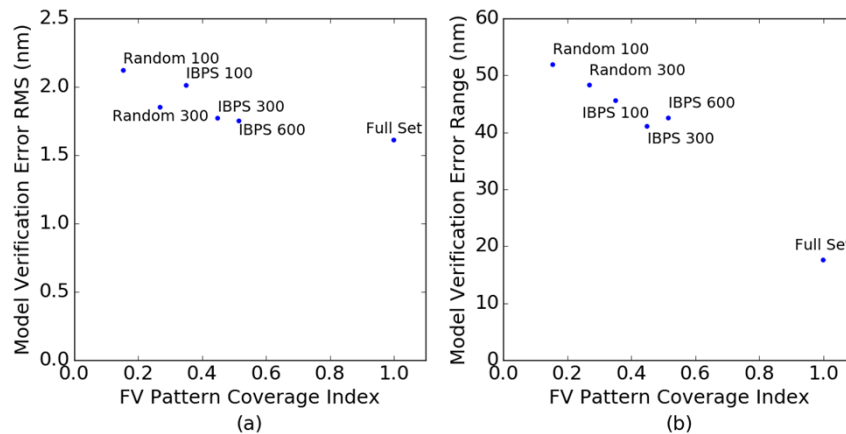

Fig. 14. Model accuracy vs FV pattern coverage index: (a) model verification error RMS vs coverage index, (b) model verification error range vs coverage index.

However, the error range is also sensitive to the minor critical patterns since the FV pattern coverage index of case Incremental 110/310 (index value is 0.351/0.447) is very similar to IBPS 100/300 (index value is 0.351/0.449) while model error range is greatly reduced in the incremental selection cases. These phenomena can only be captured by the simulation-based pattern coverage metrics, the result of which will be shown in the following section.
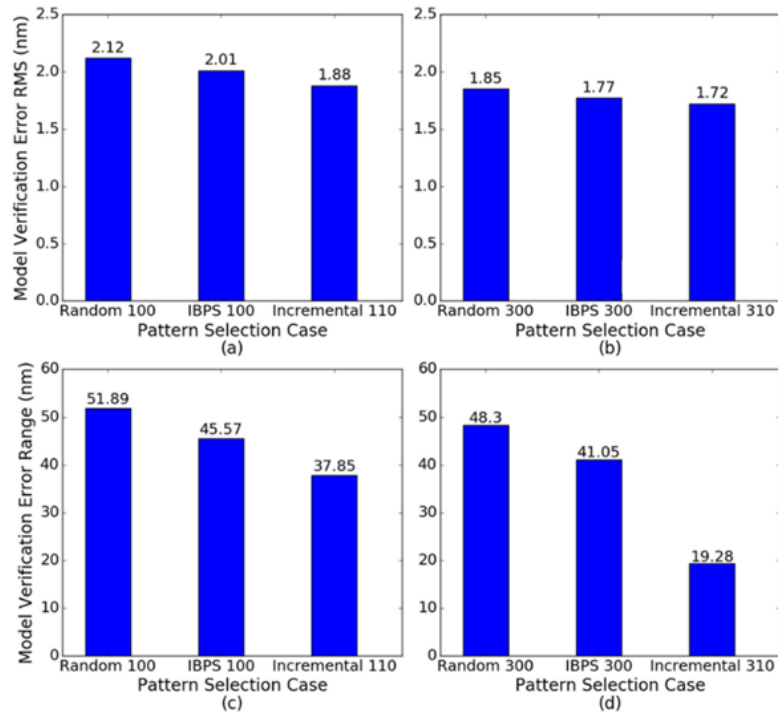
Fig. 15. Model accuracy in different cases: (a) model verification error RMS of 100 patterns, (b) model verification error RMS of 300 patterns, (c) model verification error range of 100 patterns, (d) model verification error range of 300 patterns.

4.2.　Simulation pattern coverage metrics correlate with improved model accuracy

The simulation pattern coverage result of each case is shown in Table 2. The lower range difference ratio (Range Diff Ratio) as well as the higher standard deviation ratio (Std Ratio) indicates better pattern coverage.

Table 2. Simulation-based pattern coverage result

Case ID	Random 100	IBPS 100	Incremental 110	Random 300	IBPS 300	Incremental 310
Range Diff Ratio	0.84	0.45	0.41	0.82	0.48	0.26
Std Ratio	0.69	0.86	0.98	0.74	0.96	0.96

As shown in Fig. 15, the simulation-based pattern coverage shows a strong positive correlation with the model verification error RMS and range. Under the same pattern count, the model verification error RMS/range of the IBPS set is smaller than the random selection set. This is consistent to the pattern coverage result where IBPS has better pattern coverage than random selection according to Table 2. Among all the cases, incremental pattern selection has the best pattern coverage and the smallest model verification error RMS/range. Specifically, incremental 110 has a 16.9% reduction in error range while incremental 310 reaches as large as a 53% reduction compared to IBPS 100 and IBPS 300, respectively. The results suggest that the incremental pattern selection has the capability to improve the model verification performance by further suppressing the error range whilst considering the minor critical patterns. In addition, incremental selection based on an initial selected set with larger pattern diversity, i.e., IBPS 300, tends to have more significant reduction in error range. This indicates that the diversity

of patterns selected from IBPS during the initial selection and the severity based incremental selection complements each other very well.

The model verification error distributions of each experiment case are shown in Fig. 16. According to the distribution, every model has a very good prediction on major patterns thus model verification error RMS are within or around 2 nm. The model verification error range is dominated by a few particular critical patterns with a very large verification error. The model calibrated using selected patterns with the better pattern coverage KPI shows a better prediction on these patterns, thus improving model accuracy.
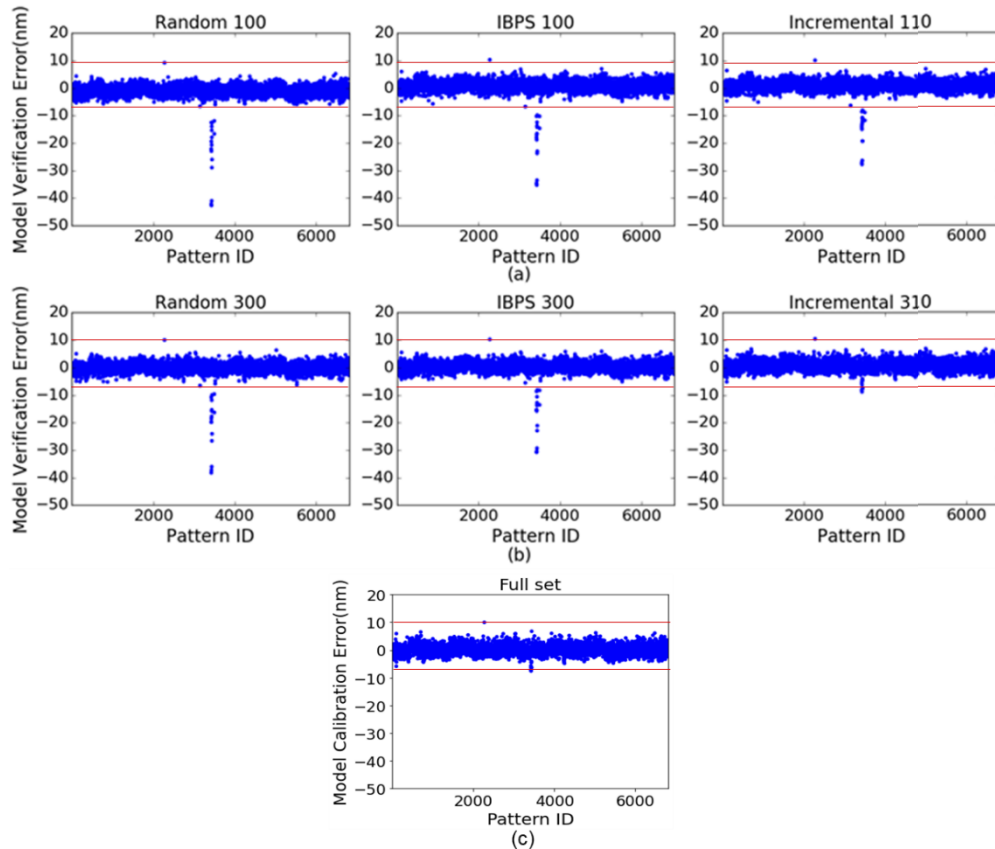

Fig. 16. Model verification error distribution: (a) 100 patterns, (b) 300 patterns, (c) full set. The large (negative) CD errors that occur on a single location are the patterns originated from the incremental selection. The upper and lower red line indicated the error range from full set.

Figure 17 shows the measured contour and the model predicted contour of two critical patterns: (a) the critical pattern found by incremental selection (referred as "Pattern A"), (b) a pattern only found in the verification set (referred as "Pattern B"). It is demonstrated that incremental selection improves the model predication accuracy not only on those used patterns but also on those unused critical patterns. Further manual analysis on the critical patterns indicates that they are much smaller in CD (critical dimension) than the majority patterns in this test case.

From Table 3, the wafer CD of Pattern A and Pattern B in the horizontal direction are 44.25 nm and 53.93 nm, respectively, while the majority patterns' wafer CD are in the range of 75 to 130 nm. From the two SEM images in Fig. 17, it is shown that the model contour extracted from Incremental 310 case follows better to the wafer contour in both Pattern A and Pattern B
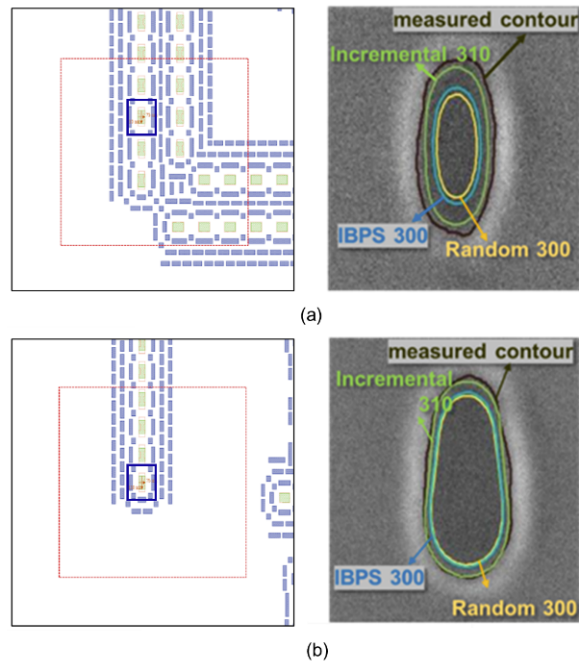
(a)

(b)

Fig. 17. Pattern design, measured and model simulated contours: (a) the critical pattern incrementally selected in 'Incremental 310' case, (b) a critical pattern only in verification set. The two SEM images are extracted from the region highlighted by the two blue boxes.

Table 3. Wafer and data of two critical patterns in three cases: Random 300, IBPS 300, and Incremental 310.

Pattern	Direction		Random 300 (nm)	IBPS 300 (nm)	Incremental 310 (nm)
Pattern A	Horizontal	Wafer CD		44.25	
		Model CD	26.53	30.50	39.90
		Model error	-17.73	-13.75	-4.36
	Vertical	Wafer CD		91.09	
		Model CD	55.06	61.78	83.42
		Model error	-36.04	-29.32	-7.67
Pattern B	Horizontal	Wafer CD		53.93	
		Model CD	43.35	44.66	52.05
		Model error	-10.58	-9.27	-1.87
	Vertical	Wafer CD		108.49	
		Model CD	92.64	95.36	108.04
		Model error	-15.85	-13.13	-0.45

compared to Random 300 and IBPS 300 cases. The model CDs of different cases are 26.53 nm (Random 300), 30.5 nm (IBPS 300), 39.9 nm (Incremental 310) for Pattern A, and 43.35 nm (Random 300), 44.66 nm (IBPS 300), and 52.05 nm (Incremental 310) for Pattern B, respectively. The much-reduced model error in Incremental 310 (Pattern A: -4.36 nm, Pattern B: -1.87 nm) compared to Random 300 (Pattern A: -17.73 nm, Pattern B: -10.58 nm) and IBPS 300 (Pattern A: -13.75 nm, Pattern B: -9.27 nm) can be ascribed to the inclusion of 10 critical patterns in

Incremental 310 case. The model results from the vertical direction, albeit is worse than that of horizontal direction, still show similar trend among all three selection. Without the inclusion of critical patterns in the calibration set, there remains some difficulty for the model to predict them well.

5. Conclusion

Pattern selection techniques and pattern coverage evaluation methods are playing increasingly important roles in lithography model calibration since they can help to reduce model calibration turn-around time and to enhance the model's accuracy. The FV based pattern coverage evaluation and simulation-based methods have been illustrated in this paper to solve the pattern coverage evaluation problem. The FV based method shows a positive relationship to model prediction accuracy with short runtime and a relatively simple flow. The simulation based method shows a strong positive correlation with the model prediction accuracy. A comparison on the characteristic of these two methods is summarized in Table 4. The simulation-based pattern coverage evaluation also enables an incremental selection method before mask tape-out and wafer metrology. It can supplement an initial selection method, e.g., IBPS, and optimize the final pattern set, which can dramatically reduce model's verification error range. Table 5 summarizes the differences between incremental selection method and the other two selection methods developed prior to this work. With both the pattern coverage evaluation and the pattern selection optimization, the OPC model calibration efficiency can be improved by reducing metrology time and the overall calibration turn-around time.

Table 4. Summary of the advantages and disadvantages of the two pattern coverage evaluation methods

Method	Principle	Advantages	Disadvantages
FV-based	Pre-defined features	Ease of use, stable, save runtime	Depends on the accuracy of AutoEncoder training
Simulation based	Model calibration	Higher accuracy, fitting result is closer to the actual error	Complex flow, need a physical model

Table 5. Comparison of the three different pattern selection methods

Selection methods	Runtime	Correlation to Model	Stability	Use Case
Random	Fast	None	Low	At any stage
IBPS	Medium	Moderate	High	Initial selection
Incremental	Slow	Strong	High	Model enhancement stage

It is worth conducting further research to enhance the correlation between FV coverage and model prediction accuracy and thus enables the qualification and optimization of selected patterns using this FV based method alone. Doing so can further reduce the turnaround time of the whole flow. Lastly, it is valuable to use the simulation-based method to verify an existing and fixed model for a new layout and to identify patterns that need special monitoring.

Disclosures. The authors declare the following competing interest: Jiaman Liu, Zhiqin Li, and Feng Yang have financial interests in Brion Technologies (Shenzhen) Co., Ltd., a subsidiary company of ASML that is focused on computational lithography and holds patents related to technologies for lithography modelling and pattern selection.

Data availability. Data underlying the results presented in this paper are not publicly available at this time but may be obtained from the authors upon reasonable request.

References

1. F. M. Schellenberg, O. Toublan, L. Capodieci, and B. Socha, "Adoption of OPC and the impact on design and layout," in *Proceedings of the 38th Design Automation Conference* (2021), pp. 89–92.
2. A. Erdmann, *Optical and EUV Lithography a Modeling Perspective* (SPIE Press, 2021).
3. Z. Wang, X. Ma, G. R. Arce, and J. Garcia-Frias, "Fast optical proximity correction method based on nonlinear compressive sensing," Opt. Express **26**(13), 16736–16751 (2018).
4. E. Y. Lam and A. K. K. Wong, "Computation lithography: Virtual reality and virtual virtuality," Opt. Express **17**(15), 12259–12268 (2009).
5. C. Mack, *Fundamental Principles of Optical Lithography: The Science of Microfabrication* (John Wiley & Sons, 2008), Chap. 2.
6. C. A. Mack, J. J. Biafore, and M. D. Smith, *MicroLithography* (CRC Press. 2020).
7. P. Liu, L.-W. Zheng, M. Ma, Q. Zhao, Y.-F. Fan, Q. Zhang, M. Feng, X. Guo, T. Wallow, K. Gronlund, R. Goossens, G. Zhang, and Y.-W. Lu, "A physical resist shrinkage model for full-chip lithography simulations," Proc. SPIE **9779**, 97790Y (2016).
8. U. K. Klostermann, T. Mülders, D. Ponomarenco, T. Schmoeller, J. V. de Kerkhove, and P. D. Bisschop, "Calibration of physical resist models: methods, usability, and predictive power," J. Micro/Nanolith. MEMS MOEMS **8**(3), 033005 (2009).
9. K. Adam, S. Ganjugunte, C. Moyroud, K. Shchehlik, M. Lam, A. Burbine, G. Fenger, and Y. Granik, "Using machine learning in the physical modeling of lithography processes," Proc. SPIE **10962**, 109620F (2019).
10. X. Ma, Q. Zhao, H. Zhang, Z.-Q. Wang, and G. R. Arce, "Model-driven convolution neural network for inverse lithography," Opt. Express **26**(25), 32565–32584 (2018).
11. Y.-S. Kim, S. Lee, and Z.-Y. Hou, *et al.*, "OPC Model accuracy study using high volume contour based gauges and deep learning on memory device," Proc. SPIE **10959**, 1095913 (2019).
12. Z.-Q. Li, L.-S. Dong, X.Y. Jing, X. Ma, and Y.-Y. Wei, "High-precision lithography thick-mask model based on a decomposition machine learning method," Opt. Express **30**(11), 17680–17697 (2022).
13. K. Lai, "Review of computational lithography modeling: focusing on extending optical lithography and design-technology co-optimization," Adv. Opt. Technologies **1**(4), 249–267 (2012).
14. R.-C. Sun, D.-K. Kang, C. Jia, M. Liu, D.-B. Shao, Y.-S. Kim, J.-H. Shin, M. Simmons, Q. Zhao, M. Feng, Y.-Q. Zhao, S.-B. Wang, S.-H. Kim, S.-W. Ko, S.-Y. Kim, J.-S. Choi, and C.-H. Park, "Enhancing model accuracy and calibration efficiency with image-based pattern selection using machine learning techniques," Proc. SPIE **11613**, 116130Y (2021).
15. L.-F. Liao, S.-K. Li, X.-Z. Wang, L.-B. Zhang, P.-Z. Gao, Y.-Y. Wei, and W.-J. Shi, "Critical pattern selection method for full-chip source and mask optimization," Opt. Express **28**(14), 20748–20763 (2020).
16. M.-C. Tsai, S. Hsu, L.-Q. Chen, Y.-W. Lu, J.-W. Li, F. Chen, H. Chen, J. Tao, B.-D. Chen, H.-Y. Feng, W. Wong, W. Yuan, X.-Y. Li, Z.-P. Li, L. Li, R. Dover, H.-Y. Liu, and J. Koonmen, "Full-chip source and mask optimization," Proc. SPIE **7973**, 79730A (2011).
17. D.-Q Zhang, G.-S. Chua, and Y.-M. Foong, *et al.*, "Source mask optimization methodology (SMO) and application to real full chip optical proximity correction," Proc. SPIE **8326**, 83261 V (2012).
18. W. Yuan, Y.-F. Lu, M. Li, B.-Y. Pan, Y. Gao, Y. Tian, Z.-Q. Li, L. Ji, Y. Huang, H. Chen, Y.-L. Yao, and S. Park, "Machine learning hotspot prediction significantly improve capture rate on wafer," in *International Workshop on Advanced Patterning Solutions* (2020), pp. 1–4.
19. Y.-B. Lin, X.-Q. Xu, J.-J. Ou, and D. Z. Pan, "Machine learning for mask/wafer hotspot detection and mask synthesis," Proc. SPIE **10451**, 104510A (2017).
20. T. Matsunawa, S. Nojima, and T. Kotani, "Automatic layout feature extraction for lithography hotspot detection based on deep neural network," Proc. SPIE **9781**, 97810 H (2016).
21. X.-L. Shi, Y.-H. Zhao, S.-M. Cheng, M. Li, W. Yuan, L. Yao, W.-H. Zhao, Y.-J. Xiao, X.-H. Kang, and A. Li, "Optimal feature vector design for computational lithography," Proc. SPIE **10961**, 109610O (2019).
22. A. K. Wong, *Optical Imaging in Projection Microlithography* (SPIE, 2005), Chap. 4.
23. S. J. Wetzel, "Unsupervised learning of phase transitions: From principal component analysis to variational autoencoders," Phys. Rev. E **96**(2), 022140 (2017).
24. M. Maggipinto, C. Masiero, A. Beghi, and G. A. Susto, "A convolutional autoencoder approach for feature extraction in virtual metrology," Procedia Manuf. **17**, 126–133 (2018).
25. X.-Y. Liu, G.-Z. Shao, Y.-W. Liu, X.-W. Liu, J.-Y. Li, X.-L. Chen, and Y.-K. Chen, "Deep classified autoencoder for lithofacies identification," IEEE Trans. Geosci. Electron. **60**, 5909914 (2022).
26. D. Holden, J. Saito, T. Komura, and T. Joyce, "Learning motion manifolds with convolutional autoencoders," in *SIGGRAPH Asia Technical Briefs* (2015), pp. 1–4.
27. V. Chvatal, "A Greedy Heuristic for the Set-Covering Problem," Math. Oper. Res. **4**(3), 233–235 (1979).
28. P. Slavík, "A Tight Analysis of the Greedy Algorithm for Set Cover," J. Algorithms **25**(2), 237–254 (1997).
29. F. X. Zach, "Neural-network-based approach to resist modeling and OPC," Proc. SPIE **5377**, 670–679 (2004).